Large-eddy simulation of turbulent combustion for gas turbines with reduced chemistry

By L. Selle†, G. Lartigue† T. Poinsot‡, P. Kaufmann¶, W. Krebs¶ AND D. Veynante‖

An LES computation has been performed for the complete burner of a partially- premixed gas turbine, for both non-reacting and reacting cases. The flame is described using a two-step chemical scheme combined with the thickened-flame (TF) model. Results show that the inlet boundary conditions (especially the swirl level) have a very large effect on flow topology. With the correct inlet conditions, the overall agreement with experiment is very good, for both cold flow and reacting flows.

1. Introduction

Large-eddy simulation (LES) is becoming a standard tool to study the dynamics of turbulent flames (see for example recent Summer Programs at CTR, the special issue of *Flow Turbulence and Combustion* (vol. 65, 2000) on LES of reacting flows, and recent books on turbulent combustion (Peters (2000)) and Poinsot & Veynante (2000)). Many recent papers have demonstrated the power of LES methods (Pierce & Moin (1998), Desjardins & Frankel (1999), Légier *et al.* (2000),5 Colin *et al.* (2000), Angelberger *et al.* (2000), Pitsch and Duchamp de Lageneste (2002)). For example, LES appears as one of the key tools for predicting and studying the combustion instabilities encountered in many modern combustion devices, such as aero or industrial gas turbines, rocket engines or industrial furnaces.

Up to now, most LES of reacting flows in complex geometries has been limited to fairly simple chemical schemes (single-step chemistry) for obvious reasons of reduction of cost and complexity. In the same way, thermodynamic and transport properties are often simplified (constant heat capacity for all species, equal Lewis numbers).

This study presents a computation of a fairly complex industrial burner, developed at Siemens Power Generation, using an unstructured LES compressible solver. The main objectives are to:

- investigate the capacities of LES in a realistic configuration,
- extend the existing flame-interaction model (called the Thickened Flame model) to a two-step chemical scheme and
- compare the LES results to experimental data obtained at University of Karlsruhe.

Section 2 presents the LES solver used for the study. The TF (Thickened Flame) model is discussed in section 3. A two-step chemical mechanism, incorporating CO as the main intermediate species, was tuned for the conditions of the Siemens burner and tested in section 4. Specific DNS were performed to check the possible effects of reduced

† CERFACS, CFD team, 42 Av. G. Coriolis, 31057 Toulouse Cedex
‡ IMF Toulouse, INP de Toulouse and CNRS, 31400 Toulouse CEDEX, France
¶ Siemens PG, Mullheim, Germany
‖ Ecole Centrale de Paris and CNRS, 92295 Châtenay Malabry CEDEX, France

chemistry on the efficiency function which characterizes the subgrid scale wrinkling in the TF model (section 5). The configuration used for the Siemens burner installed in the Karlsruhe combustion chamber is described in section 6. The specification of inlet conditions is discussed in section 7, while cold-flow results are presented in section 8. Finally, results with combustion are discussed in section 9.

2. The LES solver

The LES solver AVBP (see `www.cerfacs.fr/cfd/CFDWeb.html`) is used here. The full compressible Navier-Stokes equations are solved on hybrid (structured and unstructured) grids. Subgrid stresses are described by the WALE model (Nicoud & Ducros (1999)). The flame / turbulence interaction is modeled by the Thickened Flame (TF) model: see Angelberger *et al.* (1998), Angelberger *et al.* (2000), Colin *et al.* (2000), Légier *et al.* (2000) and Légier (2001). The numerical scheme has second- or third-order spatial accuracy and third-order time accuracy (Colin & Rydgyard(2000)). The AVBP version (AVBP 5.1) used here also handles variable heat capacities. Species enthalpies are tabulated and the mean heat capacity is determined as a function of temperature and species mass fractions Y_k. Therefore, local quantities such as the mean molecular weight W or the ratio of heat capacities γ are not constant. This introduces significant additional complexities in the numerical method, especially near boundaries, where classical characteristic methods such as NSCBC (Poinsot & Lele (1992)) must be replaced by a more complex technique (Baum, Poinsot and Thévenin (1994)).

3. The Thickened-Flame model

Modelling the interaction between flame and turbulence in partially premixed combustion systems is a major present challenge for turbulent combustion research. Possible paths are to address this issue using probability density functions (pdf) or flamelet concepts (Poinsot & Veynante (2000)). Pdf methods do not rely on any assumption on the flame topology but are limited by the accuracy of mixing models and by the required computing efforts.

On the other hand, flamelet models need assumptions for the flame topology: the flamelet approach is typically applicable when flame fronts are either of diffusion type or of premixed type. Laminar flamelet libraries are then constructed, and combined with pdf or flame-surface densities to determine species mass fractions or reaction rates in turbulent flames. When this formalism is valid, flamelet approaches offer a powerful way to incorporate complex kinetics into LES. But the flame structure type, either premixed or non-premixed, should be known *a priori* or determined from a sensor as proposed, for example, by Domingo *et al.* (2002). Unfortunately, in many practical applications such as gas turbine combustors, the flame front generally does not correspond to a pure premixed flame, separating premixed fresh gases and burnt gases perfectly, or to the usual non-premixed flame between pure fuel and pure oxidizer streams (Légier *et al.* (2000)). These situations are difficult to handle with flamelet models, even though recent work at CTR shows promising results (Pitsch and Duchamp de Lageneste (2002)).

Another path is followed here: the Thickened-Flame (TF) model initiated during the previous summer programs and continued in France (Veynante & Poinsot (1997), Angelberger *et al.* (1998), Légier *et al.* (2000), Charlette *et al.* (2002)) is now able to compute reacting flows in gas turbine combustors in complex geometries. Unsteady com-

bustion mechanisms are captured with no assumption for the flame structure: chemistry and transport are modified to offer larger reaction zones, which can be resolved on LES meshes. In this approach, the balance equation for the Y_k mass fraction in a one-dimensional flame,

$$\frac{\partial \rho Y_k}{\partial t} + \frac{\partial \rho u Y_k}{\partial x} = \frac{\partial}{\partial x}\left(\rho D_k \frac{\partial Y_k}{\partial x}\right) + \dot{\omega}_k\left(Y_j, T\right) \tag{3.1}$$

is modified as:

$$\frac{\partial \rho Y_k^{th}}{\partial t} + \frac{\partial \rho u Y_k^{th}}{\partial x} = \frac{\partial}{\partial x}\left(\rho F D_k \frac{\partial Y_k^{th}}{\partial x}\right) + \frac{1}{F}\dot{\omega}_k\left(Y_j^{th}, T^{th}\right) \tag{3.2}$$

where F is the thickening factor and superscript th stands for thickened quantities. Introducing the variable changes $X = x/F$; $\Theta = t/F$ leads to:

$$\frac{\partial \rho Y_k^{th}}{\partial \Theta} + \frac{\partial \rho u Y_k^{th}}{\partial X} = \frac{\partial}{\partial X}\left(\rho D_k \frac{\partial Y_k^{th}}{\partial X}\right) + \dot{\omega}_k\left(Y_j^{th}, T^{th}\right) \tag{3.3}$$

which has the same solution as (3.1). Then, $Y_k^{th}(x,t) = Y_k(x/F, t/F)$ showing that the flame is thickened by a factor F. The time response is also modified but this point is neglected in a first step assuming that the flame front is in equilibrium. The integrated reaction rate is kept constant:

$$\dot{\Omega}_k^{th}(t) = \int_{-\infty}^{+\infty} \frac{1}{F}\dot{\omega}_k\left(Y_j^{th}(x,t), T^{th}(x,t)\right)\, dx = \dot{\Omega}\left(\frac{t}{F}\right) \tag{3.4}$$

and, accordingly, the laminar flame speed s_L is conserved. This approach has some advantages: the flame propagation, for example, is due to the combination of diffusive and reactive terms so that quenching and ignition may be simulated. Fully-compressible equations may also be used as required to study combustion instabilities. Obvious drawbacks also exist: subgrid scale wrinkling must be modeled using an efficiency function E derived from DNS results, as shown by Veynante & Poinsot (1997), Angelberger *et al.* (1998) or Colin *et al.* (2000). Using the same DNS, a more refined efficiency function E has been recently derived by Charlette *et al.* (2002). In practice, the diffusion coefficient D_k is replaced by $E\,F\,D_k$ and the pre-exponential constant A by $A\,E/F$. The flame front is then thickened by a factor F and propagates at the subgrid-scale turbulent flame speed Es_L. Furthermore, the complexity of the chemical scheme must remain limited. Up to now, only simple one-step chemical schemes have been used. In the present study, a two-step scheme is introduced to capture CO and predict more accurate flame temperatures, as an intermediate step towards more complex schemes (typically four-step schemes such as that of Jones & Lindstedt (1988)). In fact, the approach is questionable when intermediate species are present. According to (3.4), the overall reaction rate of these species is conserved (and is close to zero), but, as the mass fraction profiles are thickened, their total amount is increased. For a one dimensional flame, this increase has no effects but could lead to some difficulties for wrinkled or/and stretched flame fronts. This point is investigated, using DNS, in section 5.

A_1	n_{1F}	n_{1O}	E_{a1}	A_2	n_{2CO}	n_{2O}	n_{2CO_2}	E_{a2}
$2E15$	0.9	1.1	34500	$2E9$	1	0.5	1	12000

TABLE 1. Rate constants for scheme 2S-CM2. The activation energies are in cal/moles and the preexponential constants in cgs units.

CH_4	CO_2	CO	O_2	H_2O	N_2
0.68	0.98	0.76	0.76	0.6	0.75

TABLE 2. Schmidt numbers used with the 2S-CM2 scheme.

4. Two-step chemistry

The chemical scheme used for this study, called 2S-CM2, takes into account six species (CH_4, O_2, CO_2, CO, H_2O and N_2) and two reactions:

$$CH_4 + \frac{3}{2}O_2 \longrightarrow CO + 2H_2O \tag{4.1}$$

$$CO + \frac{1}{2}O_2 \longleftrightarrow CO_2 \tag{4.2}$$

The first reaction (4.1) is irreversible, whereas the second one (4.2) is reversible and leads to an equilibrium between CO and CO_2 in the burnt gases. The rates of reaction (4.1) and (4.2) are given respectively by:

$$q_1 = A_1 \left(\frac{\rho Y_{CH_4}}{W_{CH_4}}\right)^{n_{1F}} \left(\frac{\rho Y_{O_2}}{W_{O_2}}\right)^{n_{1O}} \exp\left(-\frac{E_{a1}}{RT}\right) \tag{4.3}$$

$$q_2 = A_2 \left[\left(\frac{\rho Y_{CO}}{W_{CO}}\right)^{n_{2CO}} \left(\frac{\rho Y_{O_2}}{W_{O_2}}\right)^{n_{2O}} - \left(\frac{\rho Y_{CO_2}}{W_{CO_2}}\right)^{n_{2CO_2}}\right] \exp\left(-\frac{E_{a2}}{RT}\right) \tag{4.4}$$

where the parameters are given in table 1.

Transport by molecular diffusion also requires some attention: PREMIX uses polynomial fits for diffusion coefficients D_k. This technique is accurate but expensive, and may be replaced by a simpler approximation based on the observation that the individual Schmidt numbers of species $S_c^k = \nu/D_k$ are almost constant in these flames. Therefore, in AVBP 5.1, the diffusion coefficient D_k of species k is obtained as $D_k = \nu/S_c^k$ where ν is the viscosity and S_c^k the fixed Schmidt number of species k. The Schmidt number values used in the present simulations are given in table 2. In most cases, these values correspond to the PREMIX values measured in the burnt gases. The Prandtl number is set to 0.68. With this parameter set, the agreement between flame profiles obtained using AVBP 5.1 or PREMIX with the same chemical scheme is excellent.

The 2S-CM2 scheme is directly implemented into the LES code. Its first advantage compared to a single-step scheme is to provide more accurate adiabatic flame tempera-

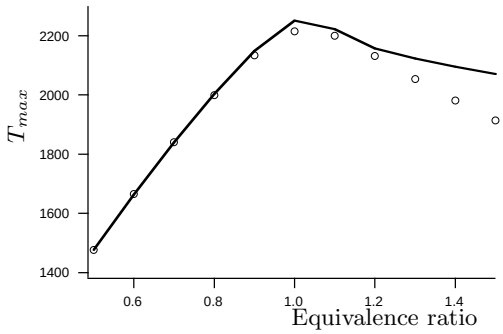

FIGURE 1. Maximum temperature T_{max} (K)
2S-CM2: ——— ; GRI mech: ○

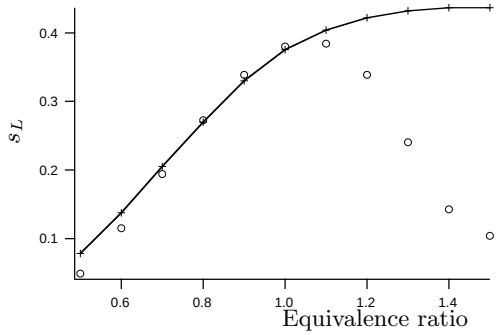

FIGURE 2. Flame speed s_L (m/s)
2S-CM2: ——— ; GRI mech: ○

tures. Figure 1 compares the maximum flame temperatures obtained with 2S-CM2 and the full GRI mech scheme. The laminar flame speeds are also well predicted on the lean side, (figure 2) but deviate from the exact results for rich cases. This drawback is not a problem for the Siemens burner investigated here: the axial burner injects pure air, while the diagonal burner feeds premixed air with an equivalence ratio of 0.5 so that combustion proceeds everywhere under lean conditions.

5. Efficiency function for reduced chemistry

The thickened-flame model is theoretically able to handle complex chemical schemes but, as described in section 3, possible drawbacks may occur because of intermediate species. Direct numerical simulations of laminar premixed flame / vortex interactions were conducted to study the thickened-flame approach combined with the 2S-CM2 chemical scheme (section 4) and to check whether the existing efficiency functions proposed by Angelberger *et al.* (1998), Colin *et al.* (2000) or Charlette *et al.* (2002) could be used without modification. This point is investigated using a pair of counter-rotating vortices interacting with a perfectly premixed flame thickened with a factor F from $F = 1$ to $F = 20$. The vortex size r is kept constant ($r/\delta_l^0 = 26.3$, where δ_l^0 is the thermal thickness of the actual laminar flame) but the vortex strength is changed (see Angelberger *et al.* (1998) or Colin *et al.* (2000) for details of the numerical configuration). A typical DNS result is displayed in figure 3. The total reaction rates of the two reactions (4.1) and (4.2) are plotted as a function of time during the interaction for various thickening factors F. The counter-rotating vortices wrinkle the flame front and increase both the flame surface and the total reaction rate. However, when the thickening factor F increases, the flame surface and the total reaction rate are underpredicted (Meneveau & Poinsot (1991)), in agreement with Angelberger *et al.* (1998) and Colin *et al.* (2000). This effect corresponds to a subgrid-scale wrinkling which must be parametrized through the efficiency function.

The main result is that the two chemical reaction rates (4.3) and (4.4) follow exactly the same evolution, although the overall quantity of carbon monoxide CO increases with increasing values of the thickening factor F. For the range of parameters investigated in the present simulations, the premixed flame acts as a flamelet distorted by the flow, even for low values of the length-scale ratio $r/(F\delta_l^0)$. No differences are found between the two reactions. Moreover, the effective strain rates induced by the vortices on the flame front, as derived from the present DNS, are in close agreement with the findings of Angelberger *et al.* (1998) and Colin *et al.* (2000). Accordingly, the efficiency functions

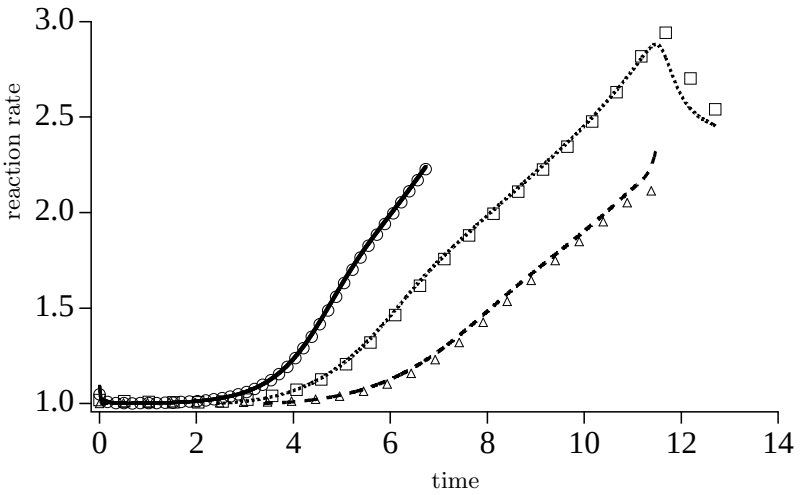

FIGURE 3. Typical flame / vortex interaction DNS results. The reduced total rates of reactions 4.1 (lines) and 4.2 (symbols) are displayed as functions of time for various thickening factors F. $F = 1$ (——— , ○); $F = 10$ (····· □); $F = 20$ (– – – – , △). Reaction rates are made non-dimensional using the reaction rate of the planar flame whereas times are reduced using the flame time δ_l^0/s_l^0. $u'/s_l^0 = 11.4$ where u' denotes the maximum vortex speed.

derived by Angelberger *et al.* (1998), Colin *et al.* (2000) and Charlette *et al.* (2002) may be used without any modifications with the present 2S-CM2 chemical scheme.

6. The Siemens burner geometry

Another objective of this study was to investigate the limits of present computer capabilities to perform LES of combustion in realistic geometries. An industrial gas turbine is considered here. The CAD data was provided by Siemens PG and meshed at CERFACS using CFD GEOM. The grid contains 306240 points and 1739695 cells. Figure 4 shows the main features of the burner: a central axial swirler (colored in dark) is used to inject and swirl air and, for certain regimes, non premixed fuel. In addition, six small tubes (not visible on this figure) can be used to generate pilot flames but they were not fed during the present computation. Most of the combustion air as well as fuel is injected by the diagonal swirler (the fuel entering through holes located on both sides of the swirlvanes). The external surface of the swirler is visualized in figure 4 by a wireframe surface.

7. Inlet conditions

As a first step, the non-reacting flow in the burner is computed and compared to LDV velocity measurements at the University of Karlsruhe. A major issue in such calculations is to specify boundary conditions. Since the axial burner flow is fully computed, the flow in Section 1a is introduced along the x axis only, without swirl. The main problem is then to specify inlet conditions for the diagonal swirler (Section 1b in figure 5). The inlet velocity profiles are adjusted to match the first measurement section in the burner under non-reacting cases. Velocity measurements have been made at various sections as shown in figure 5. The swirl velocity W and the velocity U_{22} normal to a plane parallel to the diagonal swirler exit plane (at an angle of 22 degrees compared to the vertical

FIGURE 4. Burner: the vanes of the diagonal swirler are not computed

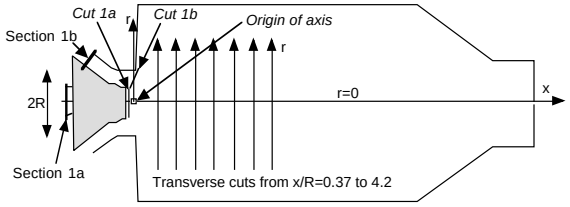

FIGURE 5. Burner mounted on ITS combustion chamber: location of LDV measurements

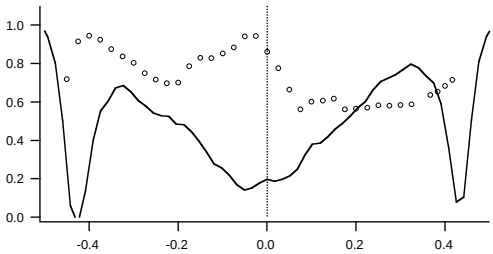

FIGURE 6. Normalized velocity U_{22}/U_{bulk} at the exit of the axial swirler (Cut 1a)
LES: ——— ; Experiments: ∘

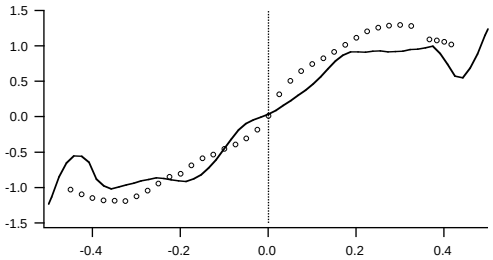

FIGURE 7. Normalized swirl velocity W/U_{bulk} at the exit of the axial swirler (Cut 1a)
LES: ——— ; Experiments: ∘

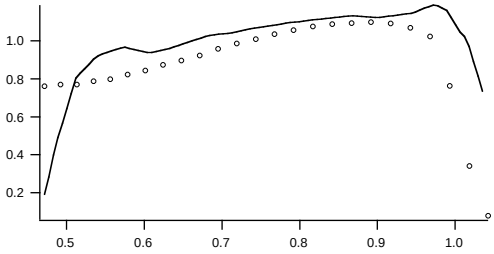

FIGURE 8. Normalized velocity U_{22}/U_{bulk} at the exit of the diagonal swirler (Cut 1b)
LES: ——— ; Experiments: ∘

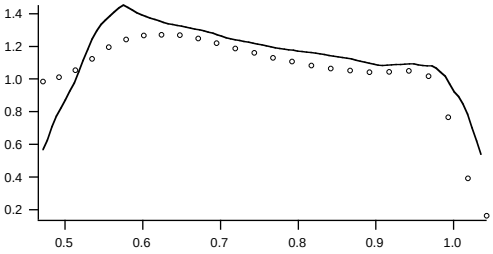

FIGURE 9. Normalized swirl velocity W/U_{bulk} at the exit of the diagonal swirler (Cut 1b)
LES: ——— ; Experiments: ∘

axis) are measured in the test section located close to the burner nozzle (cuts 1a and 1b). Distances and velocities are respectively scaled by the burner radius R and the bulk velocity U_{bulk} defined by $U_{bulk} = \dot{V}/\pi R^2$ where $\dot{V}$ is the total volume flow rate through the burner.

Average profiles of axial and radial velocities at the exit of the axial burner are shown in figure 6 and 7 (cut 1a in figure 5) and at the exit of the diagonal burner in figure 8 and 9 (cut 1b in figure 5). Measurements along cut 2 start at location R_0. In the figures, symbols (∘) denote experimental data while LES results are plotted as continuous lines.

The differences in axial velocity between LES and experimental results at the exit of

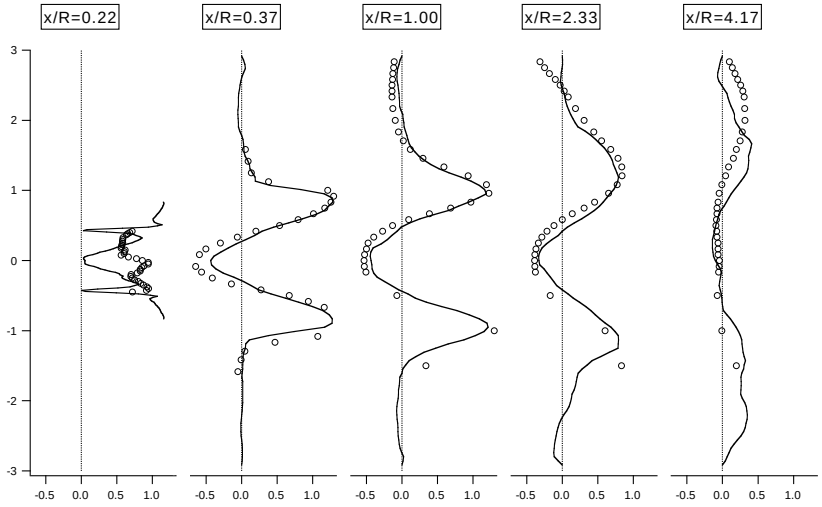

FIGURE 10. Cold flow mean axial velocities: experiment (○) and LES (———) data.

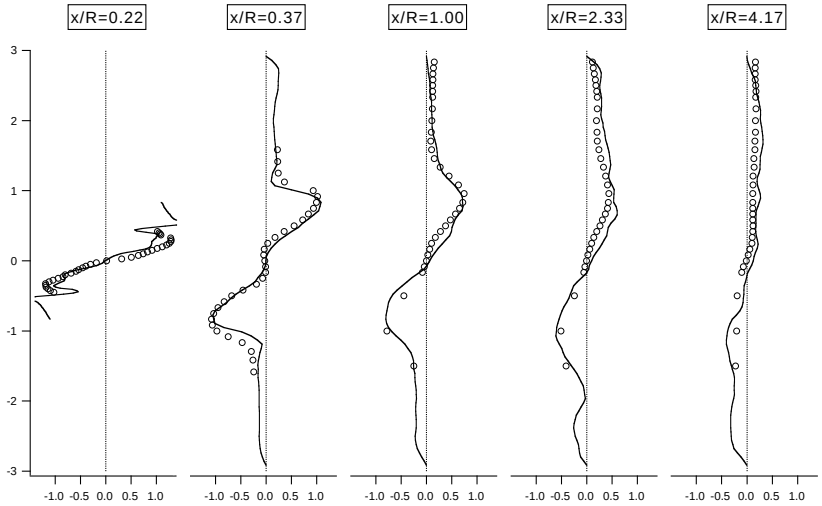

FIGURE 11. Cold flow mean swirling velocities: experiment (○) and LES (———) data.

the axial swirler (figure 6) are thought to be due to experimental uncertainties, and are being discussed with the Karlsruhe group.

8. Non-reacting flow results

Once the inlet conditions have been set, LDV measurements are compared to averaged LES results at different downstream locations x in the combustor, as shown in figures 10 (axial velocity profiles) and 11 (swirling velocities). LES results are averaged over about 36 ms corresponding to twice the flow time through the entire combustion chamber at the bulk velocity. Only five downstream locations are shown for clarity but 16 were investigated.

The overall agreement between LES and experimental data is excellent. Similar lev-

els of agreement are found for RMS values (not shown here). All results are shown for the complete combustion chamber, not just for one half chamber, to show up any departures from symmetry. Since the chamber is square and the injection device axisymmetric, average velocities are expected to be symmetrical with respect to the x-axis. Both experimental data and LES results are not symmetric, especially downstream. This finding may indicate a lack of sampling of LES data, but may also be due to an intrinsic inability of the flow to follow the symmetry of the geometry.

9. Reacting-flow results

Reacting cases are computed starting from a cold-flow solution. Fresh premixed gases (equivalence ratio $\phi = 0.5$) are injected through the diagonal swirler, while pure air is injected through the axial swirler. Both flows, which come from the compressor in the real gas turbine, enter the combustion chamber of the ITS burner after being preheated electrically. As the actual ignition process is not described here, the chemical reaction is started numerically by filling the combustion chamber with hot fully-burned gases. Note however that the pressure increases by 25 % and the exit velocity Mach number goes up to 0.4 in the outlet contraction during the transient.

Three-dimensional visualizations of the flow field are shown for five consecutive times in figure 12. A two-dimensional cut in the vertical plane at the last time is also provided, to show the fuel mass-fraction and reaction-rate fields, together with the recirculation zones. The premixed stream injected by the diagonal swirler is mixed with the pure air fed by the axial swirler and consumed by the flame front. The flame appears to be stabilized by the hot gases, both from the sides of the combustion chamber and from the recirculation zone downstream of the injector lips. A strong swirling motion is clearly apparent (rotating clockwise as seen from downstream, as in the figure. Note that a misleading analysis may be developed from two-dimensional visualizations only: the swirling motion is viewed as a flapping of the fresh reactant jets inducing "pockets" of burned gases.

Mean temperature profiles obtained from LES are compared to experimental data in figure 13. The agreement is very good: the downstream profiles, which are important for the turbine design, are very well reproduced. The slight discrepancy between experimental data and numerical results is due mainly to an underestimatden of the lateral flame expansion. This point is now under investigations: the error could be attributable to the boundary conditions.

10. Conclusions

A computation of a complete burner for a partially-premixed gas turbine combustor was performed using LES, for both non-reacting and reacting cases. The flame is described using a two-step chemical scheme, combined with the thickened-flame (TF) model which has been validated in this situation from DNS data. LES results are validated from velocity and temperature measurements obtained at the University of Karlsruhe. Results show that the inlet boundary conditions (especially the swirl level) are critical in determining the flow topology: the strength and size of the recirculation zone, and therefore the flame position, appear to be very sensitive to the profiles imposed at the diagonal swirler inlet. The overall agreement with experiment is very good, both for cold flow and for reacting conditions as long as the correct inlet conditions are imposed.

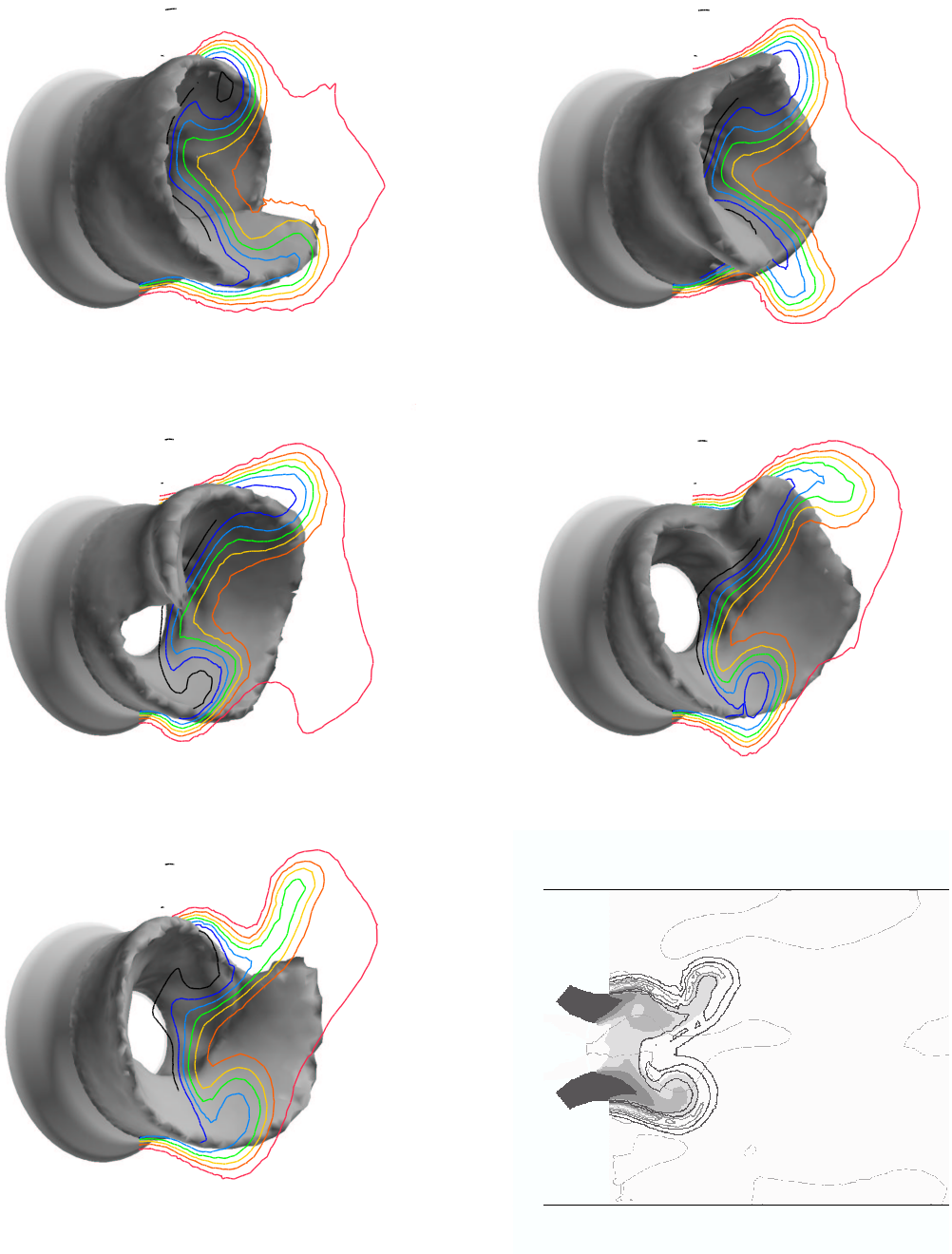

FIGURE 12. Reacting case. 3D visualizations of the reacting flow field for five consecutive times corresponding to a rotating period of the swirling flow (gray surface: fuel mass fraction; lines: temperature field in the vertical plane). A vertical 2D cut is also shown for the last time (gray scale: fuel mass fraction; bold line: reaction rate. Thin lines delineate the recirculation zones where the axial velocity is negative). Only a part of the combustion chamber is shown (zoom in the vicinity of the injector device).

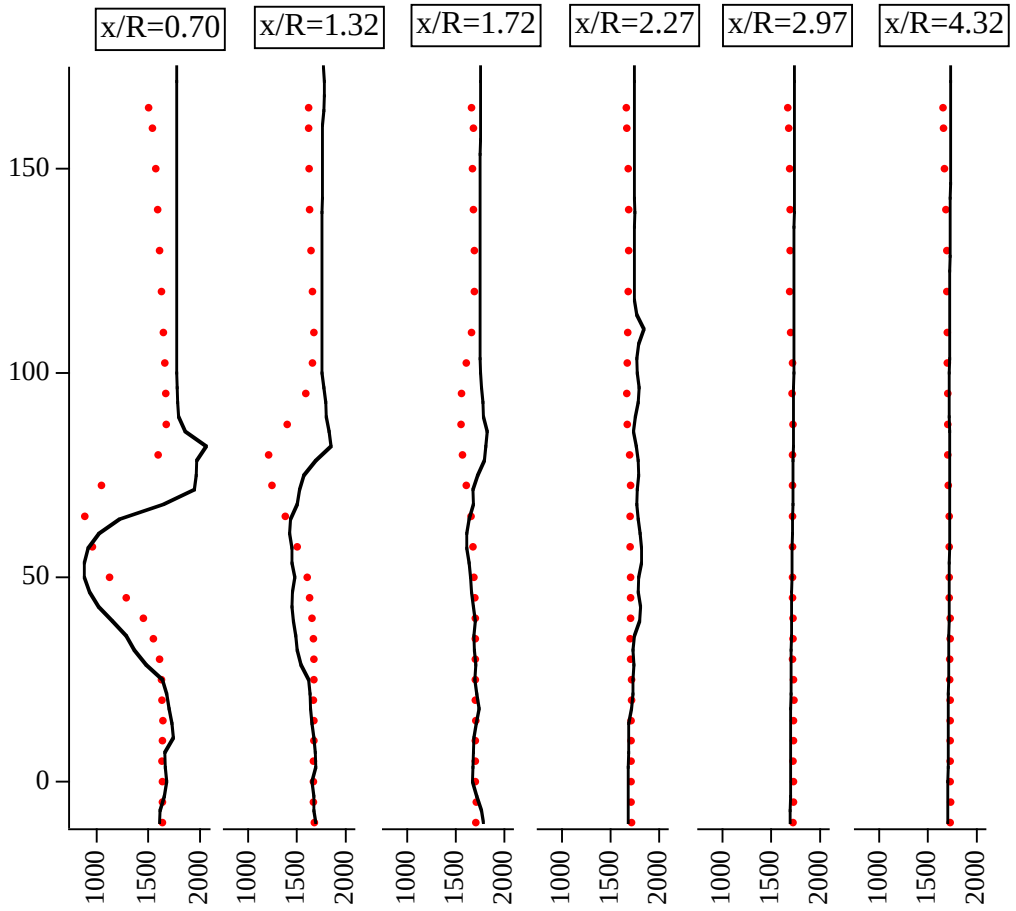

FIGURE 13. Reacting flow mean temperature: experiment (○) and LES (———) data. Measurements are conducted only in one half of the combustion chamber.

Acknowledgments

Numerical simulations have been conducted on the computers of IDRIS (Institut de Développement et de Recherche en Informatique Scientifique) and CINES French national computing centers.

REFERENCES

ANGELBERGER, C., VEYNANTE, D., EGOLFOPOULOS, F. & POINSOT, T. 1998 Large eddy simulations of combustion instabilities in premixed flames. *Proceedings of the 1998 Summer Program*, Center for Turbulence Research, NASA Ames/Stanford Univ., 61–82.

ANGELBERGER, C., EGOLFOPOULOS, F. & VEYNANTE, D. 2000 Large Eddy Simulations of chemical and acoustic effects on combustion instabilities. *Flow, Turb. and Comb.* **65**, 205-222.

BAUM, M., POINSOT, T. J. & THÉVENIN, D. 1994 Accurate boundary conditions for multispecies reacting flows *J. Comp. Phys* **116**, 247-261.

Baum, M., Thévenin, D. and Poinsot, T. Accurate boundary conditions for multicomponent reactive flows. *J. Comp. Phys.* **116**, 247–261.

Charlette, F., Veynante, D. & Meneveau, C. 2001 A power-law wrinkling model for LES of premixed turbulent combustion: Part I – non-dynamic formulation and initial tests. *Comb. and Flame*, in press.

Charlette, F., Veynante, D. & Meneveau, C. 2001 A power-law wrinkling model for LES of premixed turbulent combustion: Part II – dynamic formulation. *Comb. and Flame*, in press.

Colin, O., Ducros, F., Veynante, D. & Poinsot, T. 2000 A thickened flame model for large eddy simulations of turbulent premixed combustion. *Phys. Fluids* **12**, 1843–1863.

Colin, O. & Rudgyard M. 2000 Development of high-order Taylor-Galerkin schemes for unsteady calculations, *J. Comp. Phys.*, **162**, 2, 338–371.

Desjardins, P. E. & Frankel, S. H. 1999 Two dimensional Large Eddy Simulation of soot formation in the near field of a strongly radiating nonpremixed acetylene-air jet flame. *Comb. and Flame* **119**, 121–133.

Domingo, P., Vervisch, L., Bray, K.N.C. 2002 Modeling partially premixed flamelets in Large Eddy Simulation. *Comb. Th. Mod.*, in press.

Nicoud, F. & Ducros, F. 1999 Subgrid-scale stress modelling based on the square of the velocity gradient *Flow Turb. Comb.* **62**, 183–200.

Jones, W. P. & Lindstedt, R. P. 1988 Global reaction schemes for hydrocarbon combustion. *Comb. and Flame* **73**, 222–233.

Légier, J. P., Poinsot, T. & Veynante, D. 2000 Dynamically thickened flame Large Eddy Simulation model for premixed and non-premixed turbulent combustion.*Proceedings of the 2000 Summer Program*, Center for Turbulence Research, NASA Ames/Stanford Univ., 157–168.

Légier, J.P. 2001 Simulations numériques des instabilités de combustion dans les foyers aéronautiques. *PhD Thesis*, CERFACS, INP Toulouse.

Meneveau, C. & Poinsot, T. 1991 Stretching and quenching flamelet in premixed turbulent combustion. *Comb. and Flame* **86**, 311–332.

Peters, N. 2000 *Turbulent Combustion.* Cambridge University Press.

Poinsot, T. & Lele, S. 1992 Boundary conditions for direct simulations of compressible viscous flows. *J. Comp. Phys.* **101**, 104–129.

Poinsot, T. & Veynante, D.2001 *Theoretical and Numerical Combustion.* R.T. Edwards, Flourtown, PA.

Pierce C. & Moin, P. 1998 Large Eddy Simulation of a confined coaxial jet with swirl and heat release. *AIAA Paper* 98-2892.

Pitsch, H. and Duchamp de Lageneste, L. 2002 Large-eddy simulation of premixed turbulent combustion using a level-set approach. *Proc. 29th Sympo. on Comb.* In press.

Veynante, D. & Poinsot, T. 2000 Large Eddy Simulation of combustion instabilities in turbulent premixed burners. *Annual Research Briefs*, Center for Turbulence Research, NASA Ames/Stanford Univ., 253-274.